ACS APPLIED MATERIALS & INTERFACES

Article

Nanoporous gold as a neural interface coating: effects of topography, surface chemistry, and feature size

Christopher A. R. Chapman, Hao Chen, Marianna Stamou, Juergen Biener, Monika M Biener, Pamela Lein, and Erkin Seker

ACS Appl. Mater. Interfaces, **Just Accepted Manuscript** • Publication Date (Web): 23 Feb 2015

Just Accepted

ACS Applied Materials & Interfaces is published by the American Chemical Society.
1155 Sixteenth Street N.W., Washington, DC 20036

Nanoporous Gold as a Neural Interface Coating: Effects of Topography, Surface Chemistry, and Feature Size

*Christopher A. R. Chapman[a], Hao Chen[b], Marianna Stamou[b], Juergen Biener[c], Monika M. Biener[c], Pamela J. Lein[b], Erkin Seker[d]**

a) Department of Biomedical Engineering, University of California – Davis, Davis, CA 95616

b) Department of Molecular Biosciences, University of California – Davis, Davis, CA 95616

c) Lawrence Livermore National Laboratory, Livermore, CA 94551

d) Department of Electrical and Computer Engineering, University of California – Davis, Davis, CA 95616

ABSTRACT

Designing neural-electrode interfaces that maintain close physical coupling of neurons to the electrode surface remains a major challenge for both implantable and *in vitro* neural recording electrode arrays. Typically, low-impedance nanostructured electrode coatings rely on chemical cues from pharmaceuticals or surface-immobilized peptides to suppress glial scar tissue formation over the electrode surface (astrogliosis), which is an obstacle to reliable neuron-electrode coupling. Nanoporous gold (np-Au), produced by an alloy corrosion process, is a promising candidate to reduce astrogliosis solely through topography by taking advantage of its tunable length scale. In the present *in vitro* study on np-Au's interaction with cortical neuron-glia co-cultures, we demonstrate that the nanostructure of np-Au is achieving close physical coupling of neurons through maintaining a high neuron-to-astrocyte surface coverage ratio. Atomic layer deposition-based surface modification was employed to decouple the effect of morphology from surface chemistry. Additionally, length scale effects were systematically studied by controlling the characteristic feature size of np-Au through variations of the dealloying conditions. Our results show that np-Au nanotopography, not surface chemistry, reduces astrocyte surface coverage while maintaining high neuronal coverage, and may enhance the neuron-electrode coupling through nanostructure-mediated suppression of scar tissue formation.

KEYWORDS: Neural electrode, nanostructure, cell-material interaction, nanoporous gold, neuron-astrocyte co-culture, nanotopography, multifunctional biomaterial, gliosis

1. Introduction:

Neural-electrical interfaces (e.g. implantable electrodes and planar multiple electrode arrays) have emerged in the past decades as transformative tools to monitor and modulate neural electrophysiology for fundamental studies of the nervous system, as well as to diagnose and treat neurological disorders.[1] These interfaces require low electrical impedance to reduce background noise, and close physical coupling between the electrode and neurons for enhanced recording fidelity. An important obstacle in maintaining a robust physical neuron-electrode coupling both *in vitro* and *in vivo* is the encapsulation of the electrode by reactive glia (astrogliosis, an important contributor to scar tissue) leading to neuronal death or detachment in the vicinity of the electrode.[2-5] To that end, substantial efforts have been devoted to engineering multifunctional electrode coatings that can both maintain low electrical impedance and mitigate astrogliosis to promote strong neuron-electrode coupling.[6] Nanostructured materials[7-13] have shown promise as multifunctional coatings for neural interfaces, maintaining low impedance through large effective surface area and mitigating astrogliosis through chemical cues such as local administration of pharmacological agents[14] and surface display of immobilized peptides.[15] Very few studies have investigated the effect of topographical cues in controlling astrogliosis due in part to the complexity of studying both glia and neurons on varying surface morphologies. Ultimately, nanostructured materials for use in neural-electrical interfaces need the ability to use both chemical and topographical cues to achieve the desired tissue response. Nanoporous gold (np-Au), a nanostructured material typically produced by *dealloying* of gold-silver alloys,[16] that is, by selective dissolution of the silver component in nitric acid, enables both chemical and topographical cues to be employed to control neural tissue response. The np-Au film is composed of a network of gold ligaments and pores tens of nanometers in size (Figure 1a) with

both pores and ligaments acting as nanoscale topographical cues. Np-au has already attracted significant interest for its use in electrochemical sensors,[17-21] catalytic platforms,[17, 22] fundamental structure-property studies at the nano-scale,[21, 23-24] and tunable drug release.[25] It combines many other attractive features such as high effective surface area,[17] tunable pore size,[26] well-defined conjugate chemistry,[27] high electrical conductivity, and compatibility with traditional fabrication techniques.[28] The suitability of np-Au as a multifunctional neural electrode coating is highlighted in recent studies that demonstrate its application in high-fidelity recordings from organotypic brain slices,[29] biocompatibility,[29-31] *in situ* drug delivery for reducing astrocytic proliferation,[31] on demand drug release,[18, 32] and biofouling-resistant electrical performance.[33] Here we report the novel ability for np-Au to reduce astrocytic coverage through topographical cues. The length scale of the np-Au structure and its surface chemistry were independently controlled through altering dealloying conditions as well as ALD-based surface functionalization, respectively. This allowed us to differentiate between topographical and surface chemical effects. A primary neuron-glia co-culture model, derived from the perinatal rat neocortex, is used to accurately simulate the neural tissue environment *in vitro*.[34] We demonstrate that np-Au surface coatings dramatically reduce astrocytic surface coverage while maintaining normal neuronal coverage and show that the reduction in astrocytic coverage on the np-Au surface is in fact a function of topographical cues from the nanoscale topography and is not surface chemistry mediated.

2. Experimental Section

2.1 Sample fabrication and characterization: Samples were typically deposited in 5 mm-diameter spots onto the middle of a piranha-cleaned 12 mm-diameter thin (0.15 mm thick) glass

slide. Unstructured planar gold (pl-Au) samples were deposited by direct current sputtering (Kurt J. Lesker) of a 200 nm-thick gold layer (at 10 mTorr Ar) on top of the substrate coated with a 160 nm-thick chromium adhesion layer. Gold-silver alloy spots (precursor to np-Au) were fabricated by sputtering a 160 nm-thick chromium adhesion layer, 80 nm-thick gold corrosion barrier layer, and a 600 nm-thick gold and silver alloy (64% silver and 36% gold; atomic %). The final np-Au films were fabricated by immersing the gold-silver alloy in heated (55°C) nitric acid (70%) for 15 minutes. The short dealloying times used in the present study typically result in residual silver levels in the order of 3-5%.[25, 29] Although not necessary for this study, post treatment of the np-Au films could reduce silver levels to below 1 at.%.[35] The samples were then soaked in deionized (DI) water for one week while changing water every 24 hours. In order to produce both a high silver content np-Au film with similar feature sizes and np-Au films with increased feature sizes, the nitric acid concentration was decreased to 50% with dealloying times ranging from 10 minutes to 24 hours. **Caution:** Nitric acid is highly corrosive and reactive with organic materials and must be handled with extreme care. The morphology of the coatings was characterized by scanning electron microscopy (FEI Nova NanoSEM430), and elemental compositions before and after dealloying were assessed with energy dispersive X-ray spectroscopy (Oxford INCA, Energy-EDS). Average ligament width and pore diameter were analyzed using a custom MATLAB script by averaging both vertically and horizontally over each SEM image taken.

2.2 Cell culture and imaging: Primary rat cortical cells were obtained from the laboratory of Prof. Pamela J. Lein at University of California, Davis. All studies were conducted according to protocols approved by the Institutional Animal Care and Use Committee of the University of

California, Davis. Material samples were incubated with 0.5 mg/mL poly-L-lysine in B Buffer (boric acid and borax, Sigma, Saint Louis, MO) at 37°C in 5% CO_2 for 4 hours. Materials were then washed with sterile deionized (DI) water and then incubated for 12 hours at 37°C and 5% CO_2 with plating media consisting of 2% B27 supplement, 1X Glutamax, 10% heat-inactivated horse serum, and 1M HEPES at pH 7.5 with Neurobasal A as the basal medium (all media components were obtained from Invitrogen, Carlsbad, CA). Dissociated cortical cells were plated at a density of 50,000 cells/cm^2 on each material and kept in plating medium for 4 hours before being switched to a serum-free growth medium. Unless otherwise noted, cells were cultured for seven days to allow sufficient time for the growth and coverage of neurons and astrocytes over the material surface.[3] For cellular quantification, the cells were fixed using 4% paraformaldehyde in phosphate buffered saline (Affymetrix), and immunostained using mouse anti-tubulin-βIII antibodies (Invitrogen) to visualize neurons and rabbit anti-glial fibrillary acidic protein antibodies (GFAP, Invitrogen) to visualize astrocytes, followed by incubation with goat anti-mouse antibodies conjugated to Alexa Fluor 555 (Invitrogen) and goat anti-rabbit antibodies conjugated to Alexa Fluor 488 (Invitrogen). Counter-staining with DAPI was used to visualize cell nuclei. Images of immunostained samples were acquired using an inverted fluorescent microscope (Zeiss Observer D1). Epi-fluorescent images were analyzed using a custom ImageJ macro[28] to determine cell coverage of a given surface.

2.3 Modification of surface chemistry: Some np-Au samples were coated with 2.5 nanometer-thick Al_2O_3 films as described previously.[36] The coatings were created through the well-established trimethyl-aluminum ($AlMe_3/H_2O$) ALD process[37] in a warm wall reactor.

2.4 Statistical Methods: Each study was performed on at least three different samples per dissection, and imaged at the same five locations on each sample. Unless otherwise stated, the reported values represent averages and standard deviations of the measurements. A two-tailed Student's t-test assuming unequal variance was used to identify differences between two different sample groups. Unless otherwise noted, a one-way ANOVA was used when comparing more than two groups in each experiment. p-values less than 0.05 were deemed statistically significant.

3. Results and Discussion

The np-Au films used in this study were characterized to have an average ligament width of 30.6±1.2 nm and average pore diameter of 87.11±4.55 (Figure 1A). These feature sizes are within a range that has been shown previously to elicit cellular responses such as decreased cell adhesion and surface coverage.[13] We thus began this study by investigating the overall effect of np-Au on both neurons and astrocytes in co-culture through quantification of cell surface coverage in comparison to unstructured planar gold.

3.1 Effect of Au surface topography

In order to determine the cellular response to np-Au, the surface coverages (in percent of covered surface area) of both neuron and astrocytes on pl-Au and np-Au coatings were determined from digitally processed epi-fluorescent images (Figure 1). The neuronal surface coverage remained constant at 36% ($p > 0.9$) on both pl-Au and np-Au. However, astrocyte coverage on the np-Au surface decreased significantly ($p < 0.001$) with a 56.5% reduction in coverage from an observed 23% surface coverage on the pl-Au surface to 10% on the np-Au. This result demonstrates that

np-Au dramatically reduces astrocytic coverage over the sample surface in a cell-type selective manner (i.e. only astrocytes are affected). This observation can be extended to suggest that reduced astrocyte coverage may allow for unobstructed neuron-surface coupling on np-Au biomedical device coatings.

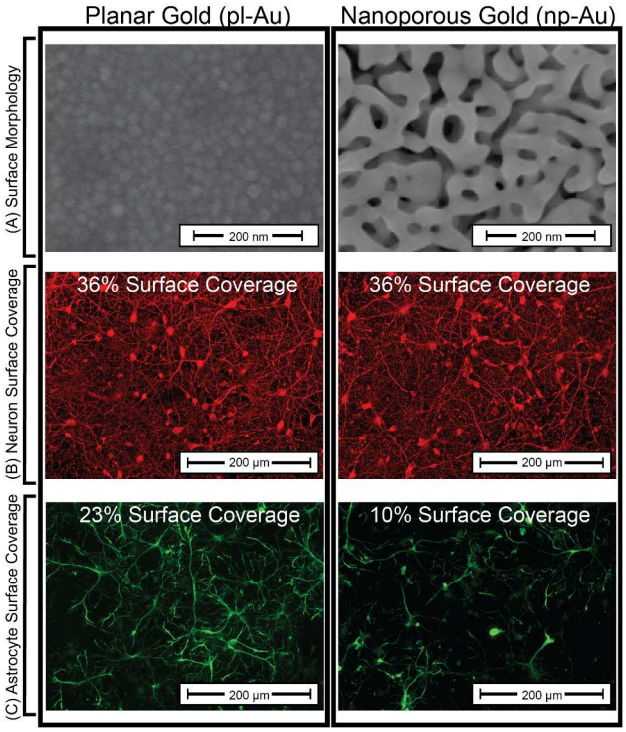

Figure 1. (A) Scanning electron micrographs of pl-Au and np-Au shows marked differences in surface morphology. (B) Fluorescent images of β-tubulin immunopositive cells (red) show high neuron coverage on both pl-Au and np-Au. (C) Fluorescent images of GFAP immunopositive cells (green) indicate significantly reduced astrocyte coverage on np-Au compared to pl-Au. Numerical values of the cell surface coverage are provided for quantitative comparison of the fluorescent images.

Although these results point towards a topographical effect, surface chemistry effects, such as residual silver in the np-Au film (either ionized into the culture medium or presented on the ligament surface) need to be ruled out as contributing factors.

3.2 Effect of residual silver

Potential cytotoxic effects of residual silver (ionized or surface-bound) were investigated by studying the effect of the residual silver content of np-Au films on both neuron and astrocyte surface coverage in neuron-glia co-cultures. For this we prepared a high-silver content np-Au film (HS np-Au) with approximately three times the residual silver content (~12 at.% instead of ~4 at.% silver). This film showed similar ligament width and pore diameter distributions as the standard np-Au film (34±1 nm and 80.78±3.2), so that any differences in cell coverage could be attributed to the effect of residual silver (Figure 2).

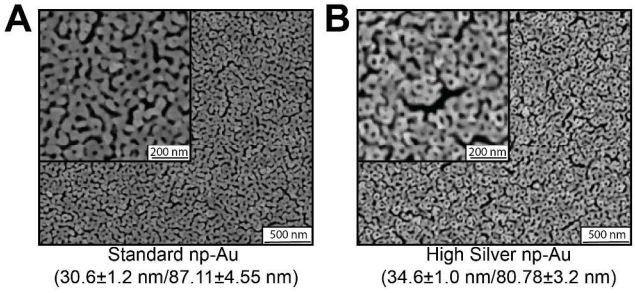

Figure 2. (A) Scanning electron micrographs of the standard (4% silver) np-Au surface and (B) the high-silver content (12% silver) np-Au surface. The low-magnification SEM micrographs demonstrate the long-range uniformity of our np-Au substrate. High magnification (100 kX) micrographs are shown in the insets, and measured ligament lengths and pore diameters are shown below.

Primary cortical neuron-glia co-cultures were grown on both standard np-Au and HS np-Au films, as well as the unstructured 64% silver precursor alloy and 0% silver unstructured pl-Au. Comparison of fluorescence microscopy images from cultures grown on the unstructured 64% silver precursor alloy and 0% pl-Au at seven days *in vitro* demonstrates a clear cytotoxic effect of silver on both neurons and astrocyte in co-culture (Figure 3A i and ii). HS np-Au films elicited cytotoxic reactions from both neurons and astrocytes with significant neuronal and astrocytic cell

death occurring in cultures grown on the HS np-Au samples, characterized by cellular morphologies consistent with apoptosis such as nuclear fragmentation and neurite fasciculation (Figure 3A iv).[38-40] Although no abnormal cellular morphologies were present at the silver amount present in the standard np-Au films, reduced astrocytic coverage was still observed (Figure 3A iii).

Although the standard np-Au film is not visually affecting the viability of neurons, these results do not rule out cytotoxic effects at the low silver levels seen in the standard np-Au film. There are two possible explanations as to why astrocytes may be more sensitive to the amount of silver on the surface than neurons: (1) astrocytes are known to sequester and excess metal ions, such as Pb and Hg, [41-42] a phenomenon thought to protect neurons; and (2) a recent study demonstrates that the proliferation of an astrocytic cell line is more susceptible to inhibition by silver nanoparticles than is a neuronal cell line.[43]

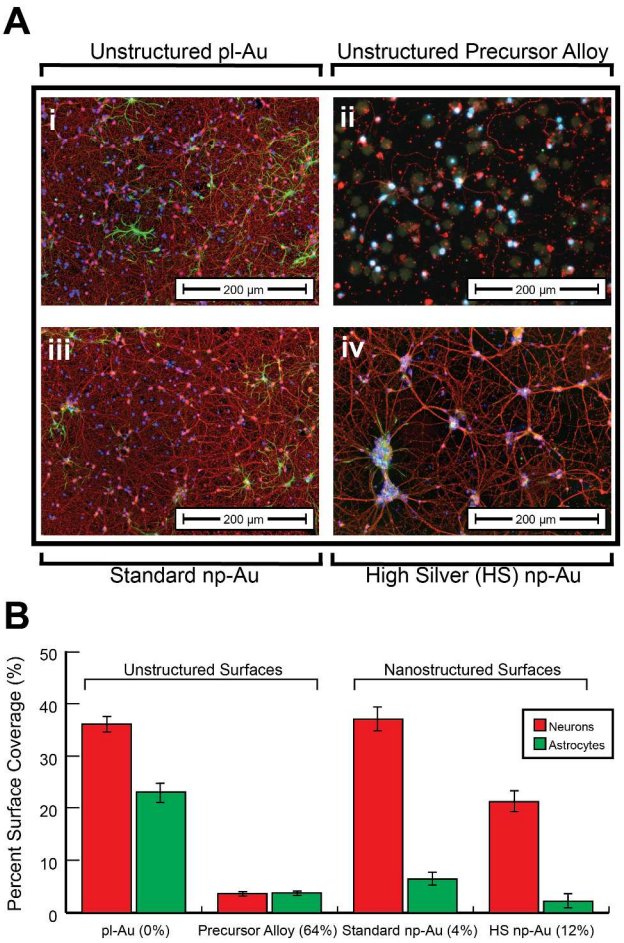

Figure 3. (A) Merged epi-fluorescent images of primary cortical neuron-glia co-cultures immunostained for β-tubulin (red – neurons) and GFAP (green – astrocytes) grown on unstructured pl-Au (i) and unstructured precursor gold-silver alloy with 64% silver (ii), as well as standard np-Au containing ~4% silver (iii) and high silver content np-Au film containing ~12% silver (iv). (B) Surface coverage analysis of day *in vitro* 7 neurons and astrocytes grown on the np-Au films containing varying amounts of silver (12% and 4%), as well as pl-Au and the gold-silver alloy reveals acute toxicity of the high silver np-Au with no visually observed toxicity of the standard np-Au.

3.3 Altering np-Au surface chemistry through ALD alumina coating

In order to further rule out potential effects from the lower amounts of residual silver typically present in the standard np-Au films, we coated standard np-Au films with conformal, 2.5 nm thick aluminum oxide (Al_2O_3) ALD films. Aluminum oxide was chosen for its biocompatibility, which has been demonstrated both *in vitro*[44] and *in vivo*[45]. The conformal coating created by ALD uniformly masks the metal surface with alumina, thereby effectively masking contained silver from any potential interaction with the cells without altering the np-Au morphology (Figure 4).[36]

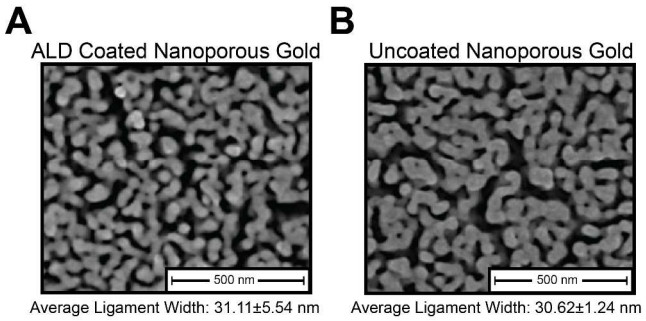

Figure 4. Scanning electron micrographs of (A) aluminum oxide-coated nanoporous gold via atomic layer deposition (ALD) and (B) uncoated nanoporous gold.

Thus the neuron-glia co-culture experiences the same nanotopography on both samples while eliminating any interaction with residual silver in the case of the ALD-coated np-Au sample. A comparison of the neuron-glia co-cultures grown on the ALD np-Au and np-Au surfaces shows similar neuron (36%) and astrocyte (10-12%) coverages (Figure 5A i-iv). This indicates that the residual silver of the standard np-Au films (i.e. 4% residual silver or less) is not the primary cause for the observed reduction in astrocytic surface coverage. To further validate this finding, pl-Au and aluminum oxide coated pl-Au (ALD pl-Au) were also tested in order to contrast the

effect of nanostructure on cortical neuron and astrocyte surface coverage. Throughout all samples, neuronal surface coverage remained constant between 35 to 37% (one-way ANOVA $p > 0.3$). Significantly reduced astrocyte surface coverage was seen on both np-Au and ALD np-Au ($p < 0.01$). Additionally, investigating astrocyte surface coverage as a function of surface chemistry alone (i.e. aluminum oxide coating) showed no significant changes between alumina and non-alumina coated pl-Au ($p > 0.5$) samples (Figure 5B).

This decoupling of the chemical cues from silver and np-Au nanotopography suggests that the reduction in astrocytic surface coverage seen on np-Au is primarily due to effects from the np-Au surface nanotopography (i.e. pores and ligaments), and not the toxicity caused by residual silver.

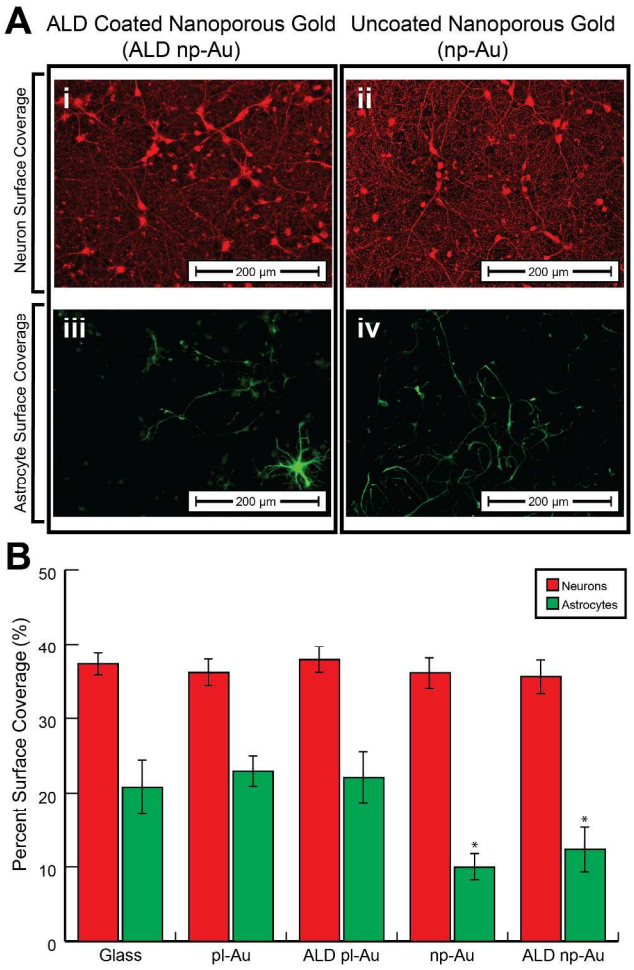

Figure 5. (A) Epi-fluorescent images of neuronal and astrocytic coverage on alumina-coated (i ,iii) and uncoated np-Au samples (ii, iv). (B) Analysis of neuron and astrocyte surface coverage on aluminum oxide-coated np-Au and pl-Au along with uncoated np-Au and pl-Au reveal that np-Au surface morphology, and not residual silver, is the dominant mechanism through which astrocyte coverage is reduced by 48-57% in comparison to pl-Au and glass. * $p < 0.001$ in comparison to pl-Au.

3.4 Mechanism of decreased astrocytic surface coverage

The observed decrease in the area of astrocyte surface coverage can be caused either by a decrease in the number of astrocytes present on the np-Au surface (astrocyte density) or solely a decrease of astrocyte cell area (surface coverage). A reduction of astrocyte number (astrocyte density) on the surface the material could indicate that this observed topographical response is cytotoxic, which is an undesirable method of reducing astrocytic surface coverage. In order to determine if the observed effect is decreasing astrocyte surface coverage through a reduction in astrocyte density or solely reducing astrocyte cell area, co-cultures were grown on standard np-Au, pl-Au, and glass to 1, 7, and 12 days *in vitro*. Astrocyte cell density (number of cells per square millimeter) was quantified between substrates. As seen in Figure 6, astrocyte cell density does not decrease over time on the np-Au substrate when compared to both pl-Au and glass.

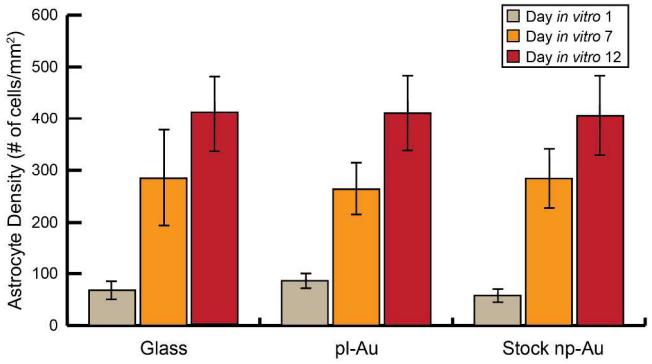

Figure 6. Quantification of astrocyte density (cells/mm^2) on glass, pl-Au, and standard np-Au surfaces at days *in vitro* 1, 7, and 12 show no significant changes in astrocyte density on standard np-Au in comparison to both pl-Au and glass substrates.

Additionally, average proliferations rates (increase in cell density per day) remained similar over each substrate for the 12-day period (Table 1).

Table 1. 12-Day Proliferation Rates [(# of cells/mm^2)/day] of Astrocytes on Different Substrates

Substrate	*Day 1-7*	*Day 7-12*	*Day 1-12*
Glass	*36.11*	*25.04*	*30.57*
pl-Au	*29.60*	*29.48*	*29.54*
Standard np-Au	*37.74*	*24.33*	*31.04*

This validates that the decrease of astrocytic surface coverage seen on the standard np-Au film is not due to a reduction in astrocyte cell density or proliferation rates (i.e. cell death), and suggests that astrocytes remain viable independent of surface coverage on the np-Au surface. This is an important result that further demonstrates the potential biocompatibility of np-Au over a time period where the most acute cytotoxicity is expected.

3.5 Feature size dependent effects

To determine if the topographic effect of np-Au substrates on the astrocytic coverage depends on the feature size of the pores and ligaments of np-Au, we fabricated a series of np-Au films with different ligament sizes (Figure 7 and Table 2), ranging from 30.6±1.24 nm for the standard np-Au (15 min - M1) to 88.61±4.89 nm (24 hour - M4). The corresponding pore diameters fell into two distinct regimes of ~87-88 nm for M1 and M2 and ~149 nm for M3 and M4.

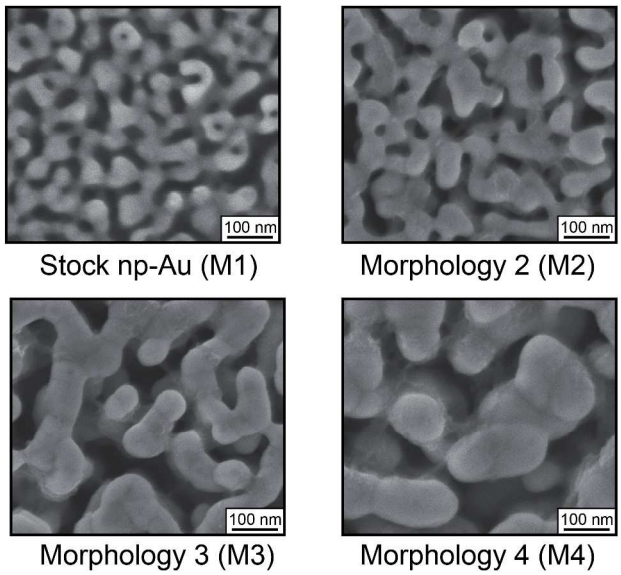

Figure 7. Scanning electron micrographs of four different np-Au surface morphologies (M1-M4) prepared by dealloying for 15 minutes to 24 hours.

Table 2. Average Ligament Widths and Pore Diameters of Fabricated np-Au Films

Film	*Ligament Width (nm)*[*]	*Pore Diameter (nm)*[*]	*Dealloying Time*
Morphology 1	*30.62±1.24*	*87.11±4.55*	*15 min*
Morphology 2	*44.54±1.01*	*88.64±5.26*	*20 min*
Morphology 3	*70.65±2.71*	*149.20±11.3*	*40 min*
Morphology 4	*88.61±4.89*	*149.24±9.9*	*24 hours*

[*] *value after "±" indicates standard error of nano-feature sizes*

Cortical neuron-glia co-cultures were then grown on each morphology for 7 days to assess feature size-dependent coverage of both neurons and astrocytes. Surface coverage analysis of both neurons and astrocytes showed a similar response to all feature sizes investigated (Figure 8). While neuronal coverage slightly increased with increasing pore and ligament size, astrocytic coverage displayed a weak non-monotonous dependence on both pore and ligament size. However, while the neuronal coverage is similar on all np-Au morphologies and pl-Au, the astrocyte coverage on np-Au remains lower than that on pl-Au, independent of the characteristic feature size of the np-Au substrate. These results shed new light on our previous work

demonstrating enhanced electrophysiological recording performance (i.e., reduced background noise and better resolved spikes) of np-Au multiple electrode arrays.[29] Reduced background noise was likely a result of reduced electrical impedance[46] stemming from the increased effective surface area of the nanoporous network; however, the 5-fold enhancement in signal strength might be due to maintaining strong neuron-electrode coupling by reducing the ionically-insulating astrocytic coverage[2,47] on the np-Au electrode surface.

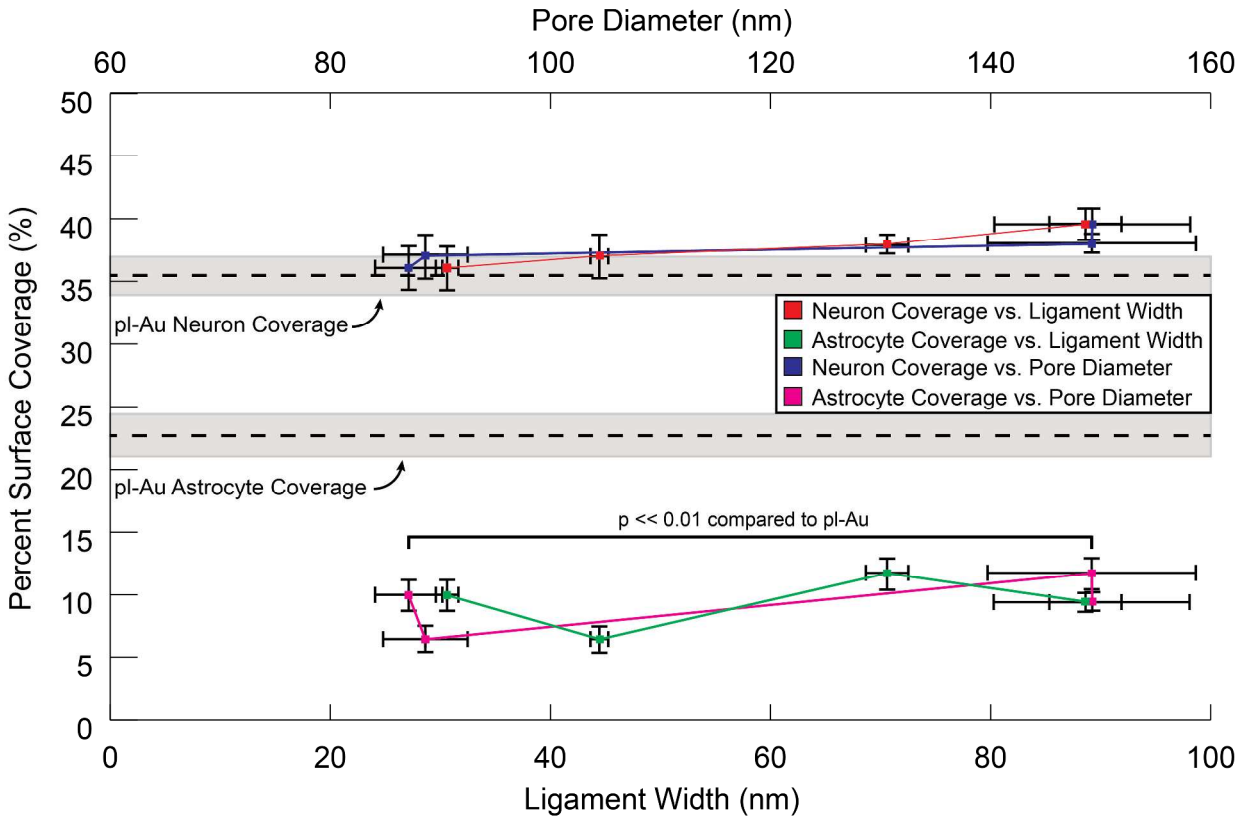

Figure 8. Quantification of neuron and astrocyte coverage vs. ligament width and pore diameter on the different np-Au surface morphologies shows a similar value for neuron coverage when compared to planar gold and a sustained decrease in astrocyte coverage on each morphology tested. The dashed horizontal lines and the shaded regions indicate mean cell coverage and its standard deviation on pl-Au respectively.

For the feature size range tested, there is no significant effect of the feature size of np-Au on the surface coverage of astrocytes and neurons. In contrast to studies that employed symmetric and uniform nanotopographical features (ordered pillars, pits, or gratings),[48] np-Au surface displays a repeatable distribution of features of varying size and shape. As shown in Table S1, even though coarsening increases average feature (i.e., ligament and pore) size, there is an overlap of feature sizes between the distributions. Therefore, the net response of a population of cells grown on np-Au can be viewed as an average response to many different features. Importantly, despite the distributions, the displayed features on np-Au are still significantly different than that on a planar gold surface (conceptualized as an infinitely-wide single ligament). The net effect is that the astrocyte coverage (despite some fluctuations as shown in Figure 8) is lower than the coverage for planar gold across different feature distributions. This study, along with others covered in the review article by Dalby et al.,[48] confirms that different cell types exhibit unique responses to varying ranges of nano-feature size. The insensitivity of neural cell response to the nanostructure sizes studies here presents possible avenues for "tuning" the morphology for other processes such as modifying drug release kinetics from the film[25] or tuning the electrical properties of np-Au films[29] without altering the cell response elicited by np-Au surface topography.

Surface effects have been shown to drive many cellular processes, including proliferation, division, migration, and adhesion. Studies involving topographical effects typically involved a single cell-type (e.g., neurons or astrocytes), which makes it difficult to simultaneously compare the responses of key neural cells. Topographical effects can influence cell response through several means; organization and spacing of integrins (critical molecules that mediate cell adhesion) along the cell membrane,[48] altering cytoskeletal formation affecting cell adhesion, as

well as intracellular signal cascades that can lead to more quiescent or reactive cell phenotypes.[49] The effect of surface roughness on different cell types has shown that cell response is highly dependent on the degree of feature size. For example, integrin clustering and cellular adhesion is significantly altered on nanoscale pits in the size range of 70 to 300 nanometers.[48] Overall, the critical "bioactive" dimensions seen in literature are generally on the order of ~50-100s of nanometers, which is in agreement with the characteristic feature sizes of the np-Au films tested in this study. As the np-Au film is obtained from a sputter-deposited thin film alloy on a flat glass surface, there is no micro-scale roughness (see Figure S1). AFM measurements of the surface roughness of the np-Au films yield a root-mean-square roughness of 8-27 nm, which is below the critical dimensions that exhibit nanotopograpy-guided apoptosis and reduced adhesion, at least for neurons.[50] This suggests that lateral geometry (as opposed to height) plays a more important role in dictating cellular response observed in this study.

High-magnification images of astrocytes grown on the np-Au surface suggest that the np-Au surface morphology inhibits the initial spreading of astrocytes across the material surface. As seen in Figure 9, visual inspection of astrocytes grown on the np-Au surface shows reduced cell diameter at day *in vitro* 1 compared to pl-Au, and fewer cellular extensions forming on np-Au at both day *in vitro* 7 and 12 compared to pl-Au (also observed for a murine astrocytic cell line by Seker *et al.* [31]). Accordingly, a possible explanation for the differential response of astrocytes and neurons to the underlying surface is related to their unique morphologies. A typical neuronal morphology includes a large proportion of thin and long processes (e.g., neurites); while a typical astrocyte has a higher ratio of thicker processes (Figure 1 and Figure 9). The random topography provided by np-Au is permissive for thin cellular processes to align along a

continuous path of ligaments and avoid the pores which may constitute discontinuities that hinder cell spreading. In agreement with this hypothesis, on the planar gold surface, astrocytes exhibit a characteristic morphology, including thick and long processes, as seen in the SEM micrograph of a murine astrocyte (Figure S2), acquired as described previously[31]. On the other hand, the np-Au surface limits the astrocytic spreading to short and thin processes (Figure S3) that align over continuous paths of ligaments (Figure S4). Since epi-fluorescent images in Figure 1 indicate no difference in neuronal surface coverage on planar gold or np-Au surfaces, it is reasonable to state that neurons with their typical morphology of long and thin neurites are not affected by the underlying surface topographies studied here. In contrast, a higher astrocytic coverage on planar gold was evident in comparison to that on np-Au, as shown in Figure 1.

Ongoing experiments investigating focal adhesion formation, as well as gene expression changes in astrocytes on np-Au surfaces, should provide further insight into dominant cellular mechanism leading to the phenomenon revealed in this paper.

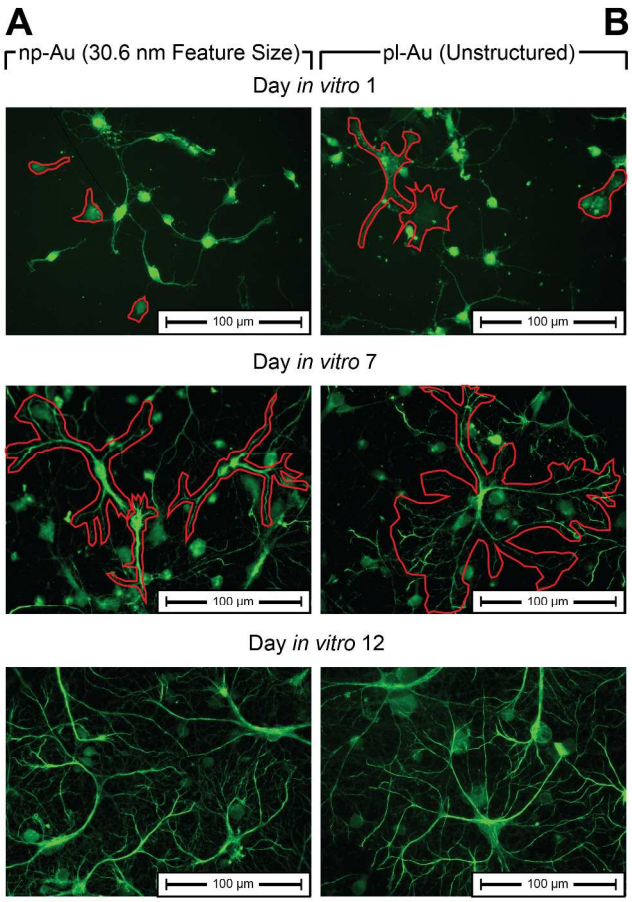

Figure 9. High magnification (40x) images of neurons and astrocytes at DIV 1, DIV 7, and DIV 12 on (A) standard np-Au and (B) unstructured pl-Au reveal cellular differences between astrocyte growth on np-Au and pl-Au. Astrocytes are highlighted by a red outline in DIV 1 and DIV 7 images. Due high non-specificity of glial fibrillary acidic protein in perinatal neurons and astrocytes, neurons are visible in DIV1 stains.[51] Astrocytes and neurons were differentiated visually through a co-localization of tubulin-β-III and GFAP (not shown here).

4. Conclusions

In conclusion, we have shown that np-Au selectively reduces astrocytic coverage while maintaining high neuronal coverage in an *in vitro* neuron-glia co-culture model. More broadly, the study demonstrates a novel surface for supporting neuronal cultures without the use of culture medium supplements to reduce glial overgrowth.[52-53] A comprehensive analysis of the

cytotoxic effects of residual silver in the np-Au films revealed that while residual silver can have an adverse effect on the viability of both neurons and astrocytes at high percentages, it is not the dominant cause for the observed selective reduction of the astrocytic surface coverage on np-Au films with less than 4% silver. This was confirmed by conformally coating the surface of np-Au with aluminum oxide to mask any possible surface chemistry effects. Thus, topographical effects from the np-Au surface morphology have been validated as the dominant mechanism that leads to a non-cytotoxic decrease in the ability of astrocytes to cover the np-Au surface. This passive reduction in astrocyte surface coverage demonstrates a non-toxic ability for np-Au to enhance the neuron-to-astrocyte surface coverage ratio in co-culture, and may allow for improved neuron-electrode physical coupling. The surface morphology-driven decrease in astrocyte coverage presents a potential avenue for np-Au electrode coatings to provide additional mitigation of adverse tissue response and enhancement of neuron-electrode coupling to np-Au-coated electrodes. Additionally, the ability for np-Au surface morphology to similarly affect astrocyte coverage in the regime from ~30-100 nanometers enables the tuning of the np-Au surface morphology for controlled release kinetic of small molecule drugs from the film.[25] This and other studies ongoing in our laboratory focus on studying histological and electrophysiological cortical cell response as a function of np-Au morphology to gain insight into the mechanisms by which morphology determines cortical cell coverage and recording fidelity. The differential effects of np-Au on astrocytic versus neuronal cell coverage reported in this study, coupled with previous demonstrations of high fidelity recordings from organoypic slices,[29] compatibility with microfabrication,[28] and reduction of astrocytic proliferation via *in situ* drug release from the np-Au patterns,[31] identify np-Au as a promising functional coating for chronic neural interfaces.

Supporting Information

Details of sample preparation, cell culture, surface functionalization, and imaging, as well as supporting scanning electron micrographs detailing effect of nanotopography on cellular response, can be found in Supporting Information. This material is available free of charge via the Internet at http://pubs.acs.org.

Corresponding Author

*Prof. Erkin Seker

Department of Electrical and Computer Engineering, University of California - Davis

1 Shields Avenue, 2064 Kemper Hall

Davis, CA 95616

Email: eseker@ucdavis.edu

Author Contributions

The manuscript was written through contributions of all authors. All authors have given approval to the final version of the manuscript.

Acknowledgements

We gratefully acknowledge the support from UC Lab Fees Research Program Award [12-LR-237197], Research Investments in the Sciences & Engineering (RISE) Award, and UC Davis College of Engineering start-up funds. C. Chapman was supported by a National Science Foundation Graduate Research Fellowship [DGE-1148897] and a predoctoral fellowship from the National Institute of Health [T32-GM008799]. Support was also provided by the

CounterACT Program, National Institutes of Health Office of the Director, and the National Institute of Neurological Disorders and Stroke [U54 NS079202]. H. Chen was supported by a predoctoral fellowship from the National Institute of Environmental Health Sciences [T32 ES007059]; H. Chen and M. Stamou received predoctoral fellowships from the Superfund Basic Research Program [P42 ES04699]. Any opinion, findings, and conclusions or recommendations expressed in this material are those of the authors(s) and do not necessarily reflect the views of the National Science Foundation or the National Institutes of Health. Work at LLNL was performed under the auspices of the U.S. DOE by LLNL under Contract DE-AC52-07NA27344.

References

1. Hochberg, L. R., Serruya, M. D., Friehs, G. M., Mukand, J. A., Saleh, M., Caplan, A. H., Branner, A., Chen, D., Penn, R. D. & Donoghue, J. P, Neuronal Ensemble Control of Prosthetic Devices by a Human with Tetraplegia. *Nature* **2006,** *442*, 164-171.
2. Polikov, V. S., Tresco, P.A. & Reichert, W.M., Response of Brain Tissue to Chronically Implanted Neural Electrodes. *J. Neurosci. Methods* **2005,** *148*, 1-18.
3. Polikov, V. S., Block, M. L., Fellous, J., Hong, J. & Reichert, W. M., In Vitro Model of Glial Scarring around Neuroelectrodes Chronically Implanted in the Cns. *Biomaterials* **2006,** *27*, 5368-5376.
4. Woolley, A. J., Desai, H. A. & Otto K. J., Chronic Intracortical Microelectrode Arrays Induce Non-Uniform, Depth-Related Tissue Responses. *J. Neural Eng.* **2013,** *10*, 1-11.
5. Ereifej, E. S., Khan, S., Newaz, G., Zhang, J., Auner, G. W. & VandeVord P. J., Characterization of Astrocyte Reactivity and Gene Expression on Biomaterials for Neural Electrodes. *J. Biomed. Mater. Res., Part A* **2011,** *99*, 141-150.
6. Fattahi, P.; Yang, G.; Kim, G.; Abidian, M. R., A Review of Organic and Inorganic Biomaterials for Neural Interfaces. *Adv. Mater.* **2014,** *26*, 1846-1885.
7. Ilic, B., Czaplewski, D., Neuzil, P., Stanczyk, T., Blough, J. & Maclay, G., Preparation of Characterization of Platinum Black Electrodes. *Am. J. Mater. Sci. Technol.* **2000,** *35*, 3447-3457.
8. Wessling, B., Besmehn, A., Mokwa, W. & Schnakenberg, U., Reactively Sputtered Iridium Oxide. *J. Electrochem. Soc.* **2007,** *154*, 83-89.
9. Bruggemann, D., Michael, K., Wolfrum, B. & Offenhausser, A., Adhesion and Survival of Electrogenic Cells on Gold Nanopillar Array Electrodes. *Int. J. Nano Biomater.* **2012,** *4*, 108-127.
10. Cui, X., Hetke, J., Wiler, J., Anderson, D. & Martin, D., Electrochemical Deposition and Characterization of Conducting Polymer Polypyrrole/Pss on Multichannel Neural Probes. *Sens. Actuators* **2001,** *93*, 8-18.
11. Wang, K., Fishman, H., Dai, H. & Harris, J., Neural Stimulation with a Carbon Nanotube Microelectrode Array. *Nano Lett.* **2006,** *6*, 2043-2048.
12. Webster, T. J., Waid, M. C., McKenzie, J. L., Price, R. L. & Ejiofor J. U., Nano-Biotechnology: Carbon Nanofibres as Improved Neural and Orthopaedic Implants. *Nanotechnology* **2004,** *15*, 48-54.
13. Kotov, N. A., Winter, J. O., Clements, I. P., Jan, E., Timko, B. P., Campidelli, S., Pathak, S., Mazzatenta, A., Lieber, C. M., Prato, M., Bellamkonda, R. V., Silva, G. A., Kam, N. W. S., Patolsky, F. & Ballerini, L., Nanomaterials for Neural Interfaces. *Adv. Mater.* **2009,** *21*, 3970-4004.
14. Spataro, L., Dilgen, J., Retterer, S., Spence, A. J., Isaacson, M., Turner, J. N. & Shain W., Dexamethasone Treatment Reduces Astroglia Responses to Inserted Neuroprosthetic Devices in Rat Neocortex. *Exp. Neurol.* **2005,** *194*, 289-300.
15. Cui, X., Wiler, J., Dzaman, M., Altschuler, R. A. & Martin, D. C., In Vivo Studies of Polypyrrole/Peptide Coated Neural Probes. *Biomaterials* **2003,** *24*, 777-787.
16. Erlebacher, J.; Aziz, M.; Karma, A.; Dimitrov, N.; Sieradzki, K., Evolution of Nanoporosity in Dealloying. *Nature* **2001,** *410*, 450-453.
17. Seker, E., Reed, M. L. & Begley, M. R., Nanoporous Gold: Fabrication, Characterization, and Applications. *Materials* **2009,** *2*, 2188-2215.
18. Santos, G. M.; Zhao, F.; Zeng, J.; Shih, W.-C., Characterization of Nanoporous Gold Disks for Photothermal Light Harvesting and Light-Gated Molecular Release. *Nanoscale* **2014,** *6*, 5718-5724.
19. Li, K., Huang, J., Shi, G., Zhang, W. & Jin, L., A Sensitive Nanoporous Gold-Based Electrochemical DNA Biosensor for *Escherichia Coli* Detection. *Anal. Lett.* **2011,** *44*, 2559-2570.
20. Feng, J., Zhao, W. & Wu, J., A Label-Free Optical Sensor Based on Nanoporous Gold Arrays for the Detection of Oligodeoxynucleotides. *Biosens. Bioelectron.* **2011,** *30*, 21-27.
21. Jin, H. J. W., J., A Material with Electrically Tunable Strength and Flow Stress. *Science* **2011,** *332*, 1179-1182.

22. Fujita, T., Guan, P., McKenna, K., Lang, X., Hirata, A., Zhang, L., Tokunaga, T., Arai, S., Yamamoto, Y., Tanaka, N., Ishikawa, Y., Asao, N., Yamamoto, Y., Erlebacher, J. & Chen, M., Atomic Origins of the High Catalytic Activity of Nanoporous Gold. *Nat. Mater.* **2012,** *11*, 775-780.
23. Hodge, A. M., Hayes, J. R., Caro, J. A., Biener, J. & Hamza, A. V., Characterization and Mechanical Behavior of Nanoporous Gold. *Adv. Eng. Mater.* **2006,** *8*, 853-857.
24. Lee, D., Wei, X., Chen, X., Zhao, M., Jun, S. C., Hone, J., Herbert, E. G., Oliver, W. C. & Kysar, J. W., Microfabrication and Mechanical Properties of Nanoporous Gold at the Nanoscale. *Scr. Mater.* **2007,** *56*, 437-440.
25. Kurtulus, O., Daggumati, P. & Seker, E., Molecular Release from Patterned Nanoporous Gold Thin Films. *Nanoscale* **2014,** *6*, 7062-7071.
26. Schade, L., Franzka, S., Mathieu, M., Biener, M. M., Biener, J & Hartmann, N., Photothermal Laser Microsintering of Nanoporous Gold. *Langmuir* **2014,** *30*, 7190-7197.
27. Bain, C. D., Troughton, E. B., Tao, Y. T., Evall, J., Whitesides, G. M. & Nuzzo, R. G., Formation of Monolayer Films by the Spontaneous Assembly of Organic Thiols from Solution onto Gold. *J. Am. Chem. Soc.* **1989,** *111*, 321-335.
28. Daggumati, P., Kurtulus, O., Chapman, C. A. R., Dimlioglu, D. & Seker, E., Microfabrication of Nanoporous Gold Patterns for Cell-Material Interaction Studies. *J. Visualized Exp.* **2013,** *e50678*.
29. Seker, E., Berdichevsky, Y., Begley, M.R., Reed, M.L., Staley, K.J. & Yarmush, M.L., The Fabrication of Low-Impedance Nanoporous Gold Multiple-Electrode Arrays for Neural Electrophysiology Studies. *Nanotechnology* **2010,** *21*, 1-7.
30. Tan, Y. H., Terrill, S.E., Paranjape, G.S., Stine, K.J. & Nichols M.R., The Influence of Gold Surface Texture on Microglia Morphology and Activation. *Biomater. Sci.* **2014,** *2*, 110-120.
31. Seker, E., Berdichevsky, Y., Staley, K.J. & Yarmush, M.L., Microfabrication-Compatible Nanoporous Gold Foams as Biomaterials for Drug Delivery. *Adv. Healthcare Mater.* **2012,** *1*, 172-176.
32. Gittard, S., Pierson, B., Ha, C., Wu, C., Narayan, R. & Robinson D., Supercapacitive Transport of Pharmacologic Agents Using Nanoporous Gold Electrodes. *Biotechnol. J.* **2010,** *5*, 192-200.
33. Patel, J., Radhakrishnan, L., Zhao, B., Uppalapati, B., Daniels, R.C., Ward, K.R. & Collinson M.M, Electrochemical Properties of Nanostructured Porous Gold Electrodes in Biofouling Solutions. *Anal. Chem.* **2013,** *85*, 11610-11618.
34. Wayman, G. A., Impey, S., Marks, D., Saneyoshi, T., Grant, W. F., Derkach, V. & Soderling, T. R., Activity-Dependent Dendritic Arborization Mediated by Cam-Kinase I Activation and Enhanced Creb-Dependent Transcription of Wnt-2. *Neuron* **2006,** *50*, 897-909.
35. Erlebacher, J., Aziz, M. J., Karma, A., Dimitrov, N. & Sieradzki, K., Evolution of Nanoporosity in Dealloying. *Nature* **2001,** *410*, 450-453.
36. Biener, M. M., Biener, J., Wichmann, A., Wittstock, A., Baumann, T., Baumer, M. & Hamza, A., Ald Functionalized Nanoporous Gold: Thermal Stability, Mechanical Properties, and Catalytic Activity. *Nano Lett.* **2011,** *11*, 3085-3090.
37. George, S. M., Atomic Layer Deposition: An Overview. *Chem. Rev.* **2010,** *110*, 111-131.
38. Howard, A. S., Fitzpatrick, R., Pessah, I., Kostyniak, P. & Lein, P. J., Polychlorinated Biphenyls Induce Caspase-Dependent Cell Death in Cultured Embryonic Rat Hippocampal but Not Cortical Neurons Via Activation of the Ryanodine Receptor. *Toxicol. Appl. Pharmacol.* **2003,** *190*, 72-86.
39. Arends, M. J., Morris, R. G. & Wyllie, A. H., Apoptosis. The Role of the Endonuclease. *Am. J. Pathol.* **1990,** *136*, 593-608.
40. Lonze, B. E., Riccio, A., Cohen, S. & Ginty, D. D., Apoptosis, Axonal Growth Defects, and Degeneration of Peripheral Neurons in Mice Lacking Creb. *Neuron* **2002,** *34*, 371-385.
41. Zalups, R. K. K. J., *Molecular Biology and Toxicology of Metals*. Taylor & Francis Inc: 2000; Vol. 1, p 609.
42. Squire, L. R., Berg, D., Bloom, F.E., du Lac, S., Ghosh, A. & Spitzer, N.C., *Fundamental Neuroscience*. Academic Press: 2008; Vol. 4.

43. Huang, C. L., Hsiao, I. L., Lin, H. C., Wang, C. F., Huang Y. J. & Chuang, C. Y., Silver Nanoparticles Affect on Gene Expression of Inflammatory and Neurodegenerative Responses in Mouse Brain Neural Cells. *Environ Res.* **2015,** *136*, 253-263.
44. Bruggemann, D., Nanoporous Aluminium Oxide Membranes as Cell Interfaces. *J. Nanomater.* **2013,** *2013*, 1-18.
45. Boutin, P., Christel, P., Dorlot, J. M., Meunier, A., de Requancourt, A., Blanquaert, D., Herman, S., Sedel, L. & Witvoet, J., The Use of Dense Alumina-Alumina Ceramic Combination in Total Hip Replacement. *J. Biomed. Mater. Res.* **1988,** *22*, 1203-1232.
46. Ludwig, K. A., Uram, J. D., Yang, J., Martin, D. C. & Kipke D. R., Chronic Neural Recordings Using Silicon Microelectrode Arrays Electrochemically Deposited with a Poly(3,4-Ethylenedioxythiophene) (Pedot) Film. *J. Neural Eng.* **2006,** *3*, 59-70.
47. Spira, M. H., A., Multi-Electrode Array Technologies for Neuroscience and Cardiology. *Nat. Nanotechnol.* **2013,** *8*, 83-94.
48. Biggs, M. J. P., Richards, R. G. & Dalby, M. J., Nanotopographical Modification: A Regulator of Cellular Function through Focal Adhesions. *Nanomedicine* **2010,** *6*, 619-633.
49. Morgan, J. T., Murphy, C. J. & Russell, P., What Do Mechanotransduction, Hippo, Wnt, and Tgfb Have in Common? Yap and Taz as Key Orchestrating Molecules in Ocular Health and Disease. *Exp. Eye Res.* **2013,** *115*, 1-12.
50. Brunetti, V., Maiorano, G., Rizzello, L., Sorce, B., Sabella, S., Cingolani, R. & Pompa, P. P., Neurons Sense Nanoscale Roughness with Nanometer Sensitivity. *PNAS* **2010,** *107*, 6264-6269.
51. Garcia, A. D. R., Doan, N. B., Imura, T., Bush, T. G. & Sofroniew, M. V., Gfap-Expressing Progenitors Are the Principal Source of Constitutive Neurogenesis in Adult Mouse Forebrain. *Nat. Neurosci.* **2004,** *7*, 1233-1241.
52. Billingsley, M. M., H., Effects of DNA Synthesis Inhibitors on Post-Traumatic Glial Cell Proliferation. *J. Pharmacol. Exp. Ther.* **1982,** *222*, 765-770.
53. Dyhrfjeld-Johnsen, J., Berdichevsky, Y., Swiercz, W., Sabolek, H. & Staley, K., Interictal Spikes Precede Ictal Discharges in an Organotypic Hippocampal Slice Culture Model of Epileptogenesis. *J. Clin. Neurophysiol.* **2010,** *27*, 418-424.

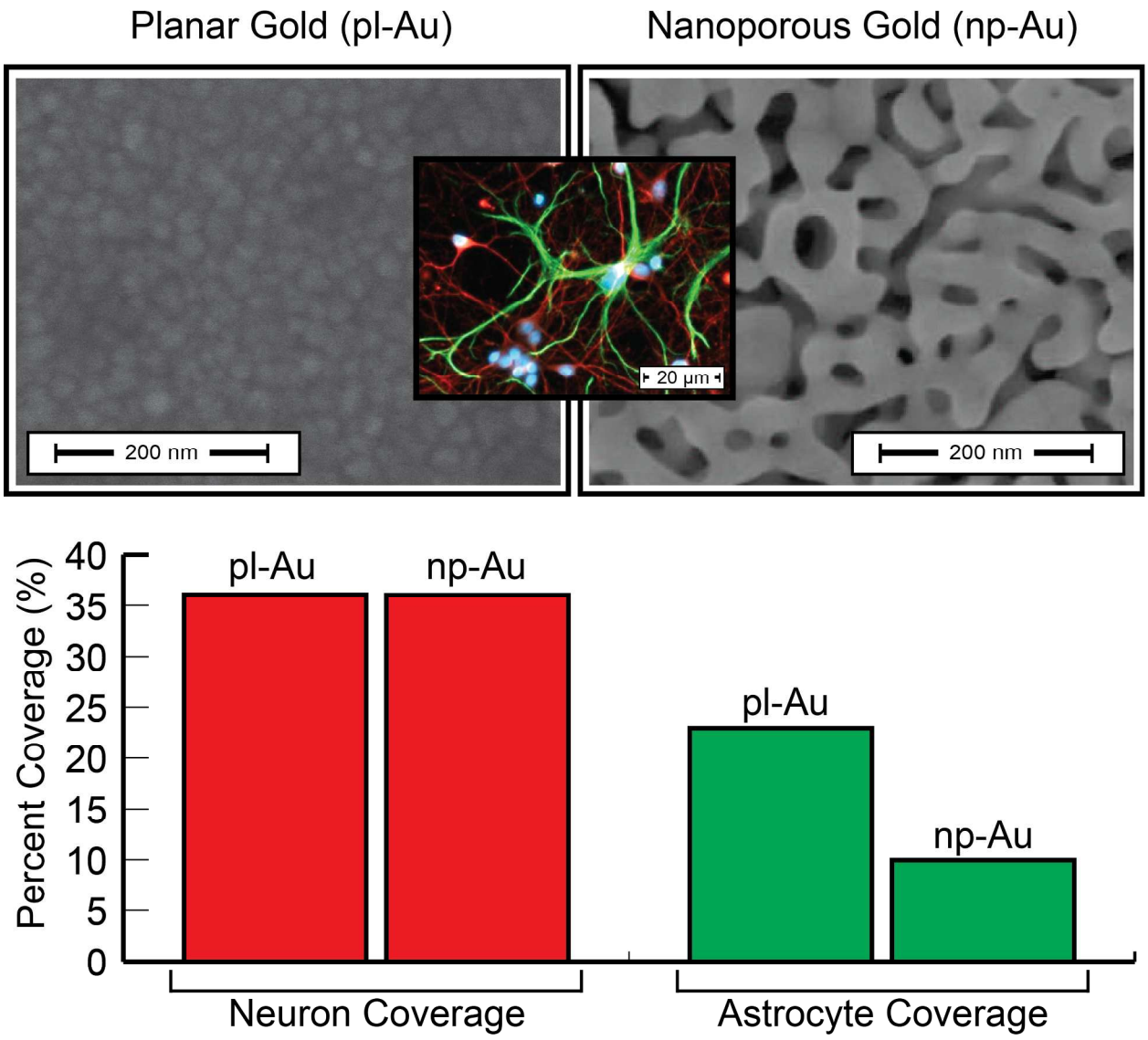
Planar Gold (pl-Au)
Nanoporous Gold (np-Au)
200 nm
20 μm
200 nm
Percent Coverage (%)
40
35
30
25
20
15
10
5
0
pl-Au
np-Au
pl-Au
np-Au
Neuron Coverage
Astrocyte Coverage

Supporting Information

Nanoporous Gold as a Neural Interface Coating: Effects of Topography, Surface Chemistry, and Feature Size

Christopher A. R. Chapman[a], Hao Chen[b], Marianna Stamou[b], Juergen Biener[c], Monika Biener[c], Pamela J. Lein[b], Erkin Seker[d]*

a) Department of Biomedical Engineering, University of California – Davis, Davis, CA 95616

b) Department of Molecular Biosciences, University of California – Davis, Davis, CA 95616

c) Lawrence Livermore National Laboratory, Livermore, CA 94551

d) Department of Electrical and Computer Engineering, University of California – Davis, Davis, CA 95616.

[*]Corresponding author e-mail: eseker@ucdavis.edu

1. Experimental Details

Chemicals and Materials: Thin (0.15 mm-thick) glass coverslips (12 mm-diameter), used as substrates for film deposition, were purchased from Electron Microscopy Sciences. Gold, silver, and chrome targets (99.95% pure) were obtained from Kurt J. Lesker. Polydimethylsiloxane (PDMS) sheets were obtained from B&J rubber products. Isopropyl alcohol, nitric acid (70%, used as received), boric acid, and borax were purchased from Sigma-Aldrich. Sulfuric acid (96%) and hydrogen peroxide (30%) were obstained from J. T. Baker. Piranha solution, for cleaning glass substrates consisted of 1:4 ratio (by volume) of hydrogen peroxide and sulfuric acid.

Sample Preparation and characterization: Glass coverslips were cleaned by oxygen plasma exposure (Harrick Plasma Cleaner) for 60 seconds at 10 W and subsequently immersed in freshly-prepared piranha solution for 10 minutes. The coverslips were then rinsed using deionized (DI) water and dried under nitrogen. PDMS stencil masks with 5 mm-diameter spots were prepared using a laser cutter (VersaLaser, Universal Laser System). The stencil masks were then cleaned with isopropyl alcohol and dried under nitrogen flow. Piranha cleaned coverslips were aligned over the stencil with the sample surface facing the stencil. The stencil was then mounted onto a 4-inch wafer using before being loaded into the sputtering machine (Kurt J. Lesker) for sequential deposition of metals. First, a 160 nm-thick chrome layer was sputtered at 300 W as an adhesive layer between the glass substrate and the subsequent metal layers. Next, 80 nm of gold was sputtered at 400 W as a seed layer to reinforce the porous coating. Finally, silver and gold were co-sputtered at 100 W and 200 W respectively. All depositions were performed under argon atmosphere at 10 mTorr. All films fabricated for this study presented a final stack

size of ~1 micrometer and an alloy thickness of ~600 nm. Prior to dealloying the precursor AuAg alloy to produce np-Au films, the samples were treated with oxygen plasma for 60 seconds at 10 W and then immersed in heated nitric acid for 15 minutes at 55 °C. Following dealloying, samples were rinsed with DI water three times and stored in DI water for one week while replacing the water every day. Before use, the samples were dried under nitrogen flow. In order to produce both a high silver content np-Au film with similar ligament widths and np-Au films with increased ligament width, both the dealloying time and nitric acid concentration were altered. Films were created using diluted nitric acid (50%) at 55°C while altering the dealloying times. The high silver np-Au film was produced from a 10 minute dealloying, and was characterized to have ~12% (atomic percent) silver after production. Longer dealloying times of 20 minutes, 40 minutes, and 24 hours unheated were used to produce np-Au films with 37%, 79%, and 97% increased ligament widths respectively. The bulk residual silver content was then analyzed using energy dispersive X-ray spectroscopy (EDS, Oxford INCA) and scanning electron microscopy (FEI Nova NanoSEM430) at 50 kX for each sample produced. Top view images of samples were analyzed using a custom ImageJ (NIH freeware) macro and a custom MATLAB script to quantify morphological differences between films through comparing average ligament width and pore diameter. Briefly, the gray-scale SEM images were segmented into monochrome images in order to define pore as black and ligaments as white. A MATLAB script was then used to calculate the average width of the black features (ligaments) and white features (pore diameters) by taking pixel intensity slices along nine lines through each image.

Sample preparation and imaging for cell culture: Previously prepared samples were treated with oxygen plasma exposure for 60 seconds at 10 W. Samples were then placed in 24 well plates

(Corning) and transferred to a sterile environment. 500 mL of 0.5 mg/mL poly-L-lysine (PLL) solution was pipetted onto each sample. This PLL solution consists of poly-L-lysine, boric acid, borax, and water adjusted to a final pH of 8.5 (Sigma Aldrich). Samples were incubated with the PLL solution for 4 hours at 37 °C and 5% CO_2 before being washed with deionized water 6 times for 1 minute each wash. After washing, 500 mL of plating media were pipetted onto the samples. Plating media consists of 2% B27 supplement, 1X Glutamax, 10% heat-inactivated horse serum, and 1M HEPES at pH 7.5 with Neurobasal A as the basal medium. Samples were incubated with plating medium for 12 hours at 37 °C in a 5% CO_2 incubator. Primary cortical rat cells were obtained from the laboratory of Dr. Pamela Lein at the University of California, Davis following a procedure seen in Wayman, *et al*.[34] Cells were counted and suspended into plating medium at the desired density. The plating medium was aspirated from the samples and the cells were plated onto the samples at a density of 50,000 cells/cm^2. Cells were incubated for 4 hours at 37 °C and 5% CO_2 with plating media in order to promote attachment. After 4 hours, the plating media was aspirated and replaced with 500 mL of a serum free growth media (growth medium consists of 2% B27 supplement and 1x Glutamax with Neurobasal A as the basal medium). The cultures were grown for 7 days *in vitro* while supplementing with fresh growth medium at day 4 *in vitro*. At day *in vitro* 7 the cultures were fixed by washing 3 times with phosphate buffered saline (PBS) and subsequent incubation with 4% paraformaldehyde in PBS for 30 minutes at room temperature. Samples were then washed 3 times with PBS and stored at 4 °C until further processed. Before staining, samples were washed twice for 5 minutes using 0.05% Tween20 in PBS containing calcium and magnesium ions (PBS[+]). The cultures were then permeabilized using 0.1% Triton X-100 in PBS[+] for 3 minutes and washed twice more with 0.05% Tween20 for 5 minutes each wash. After that, samples were blocked with 2% goat serum in PBS[+] for 30

minutes at room temperature. A primary antibody solution of 10 μg/mL of mouse anti-tubulin-βIII and 100 μg/mL of rabbit anti-GFAP was prepared with a base of blocking buffer (2% goat serum in PBS[+]). After aspirating the blocking buffer from the samples, 80 μL of primary antibody solution was transferred to the sample surface and incubated for 1 hour at room temperature. After 1 hour the primary antibody solution was removed and samples washed three times with 0.05% Tween20 in PBS[+], 5 minutes for the first two and 10 minutes for the final wash. Secondary antibody solution consisting of goat anti-mouse conjugated to AlexaFluor 555 and goat anti-rabbit conjugated to AlexaFluor 488 at dilutions of 20 μg/mL was prepared in a base of PBS[+]. After washing, 80 μL of the secondary antibody solution was transferred to the surface of each sample and incubated in the dark for 1 hour at room temperature. Samples were then washed three times using PBS[+] and 80 μL of 4',6-diamidino-2-phenylindole (DAPI; nuclear stain) solution at a dilution of 1:20000 was applied. Finally, samples were washed three times with 0.05% Tween20 in PBS[+], rinsed in TC grade water, and mounted to number 1.5 glass slides (24 mm x 60 mm, Ted Pella) using Fluoroshield mounting agent (Sigma). Samples were imaged using an inverted fluorescent microscope (Zeiss Observer D1). Images were taken using a 100x objective in five predetermined fields on each sample to account for variability in each culture. Analysis of neuron and astrocyte surface coverage (percent coverage of cells in unit surface area) was performed on co-cultures grown on glass, planar gold (pl-Au) and nanoporous gold, as well as aluminum oxide-coated planar gold and nanoporous gold. The images were analyzed using ImageJ (NIH freeware) to calculate cell coverage.

Atomic layer deposition on nanoporous gold samples: The np-Au samples were ALD coated with nanometer-thick Al_2O_3 films using the well-established trimethyl-aluminum ($AlMe_3/H_2O$) ALD process[48] in a warm wall reactor (wall temperature of 100 ^oC and stage temperature of

125 ^{o}C). This process is ideally suited to coat high aspect ratio materials such as np-Au due to the high volatility of the $AlMe_3$ precursor. Static dosing conditions (during which the chamber was isolated from the vacuum line) and long exposure and purge times (200 seconds each) were used to ensure uniform coatings throughout the porous material. The growth rate per cycle was calculated from the measured mass gain and the known surface area of bulk np-Au. Typically we used 10 ALD cycles corresponding to a film thickness of a 2.5 nm.

2. Figures and Tables

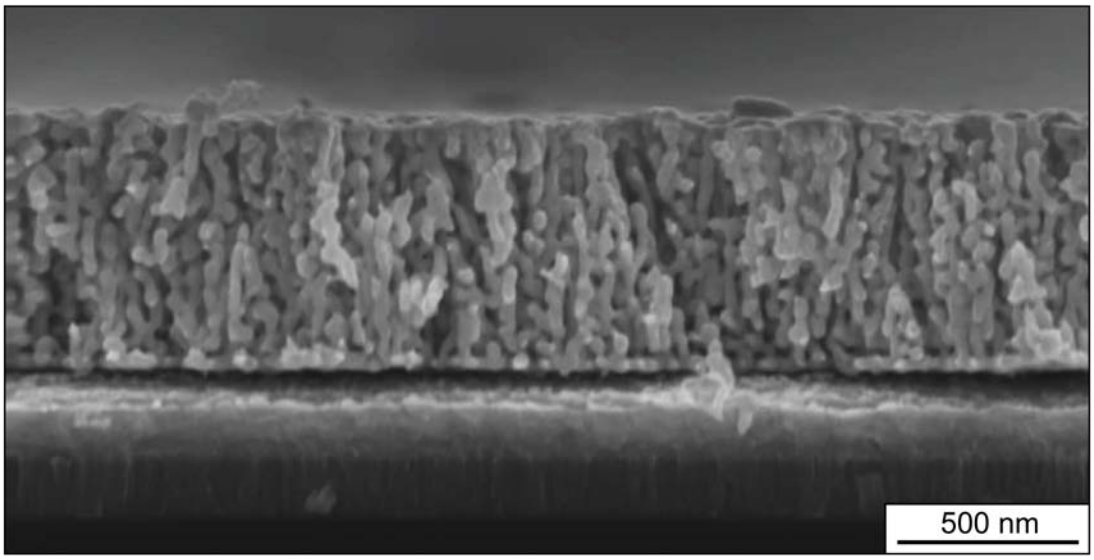

Figure S1. The cross-sectional image of np-Au reveals flat surface with minimal roughness.

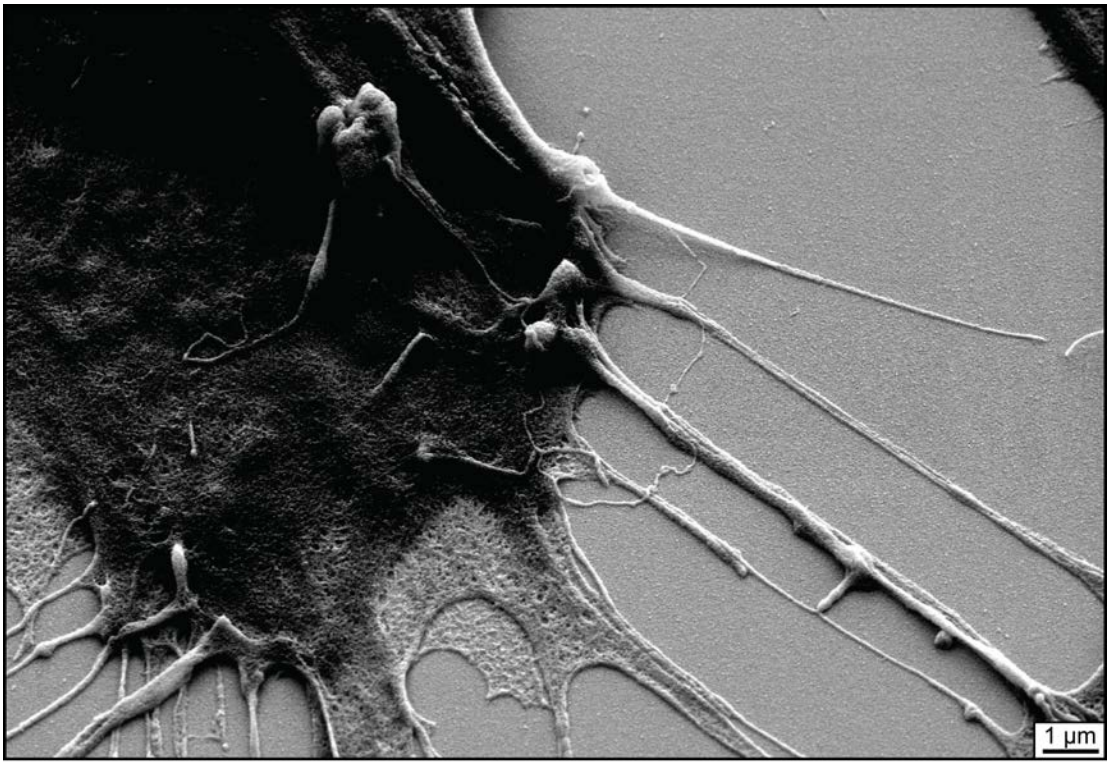

Figure S2. The SEM image illustrates typical astrocyte morphology on a planar gold surface, displaying characteristic thick and long processes.

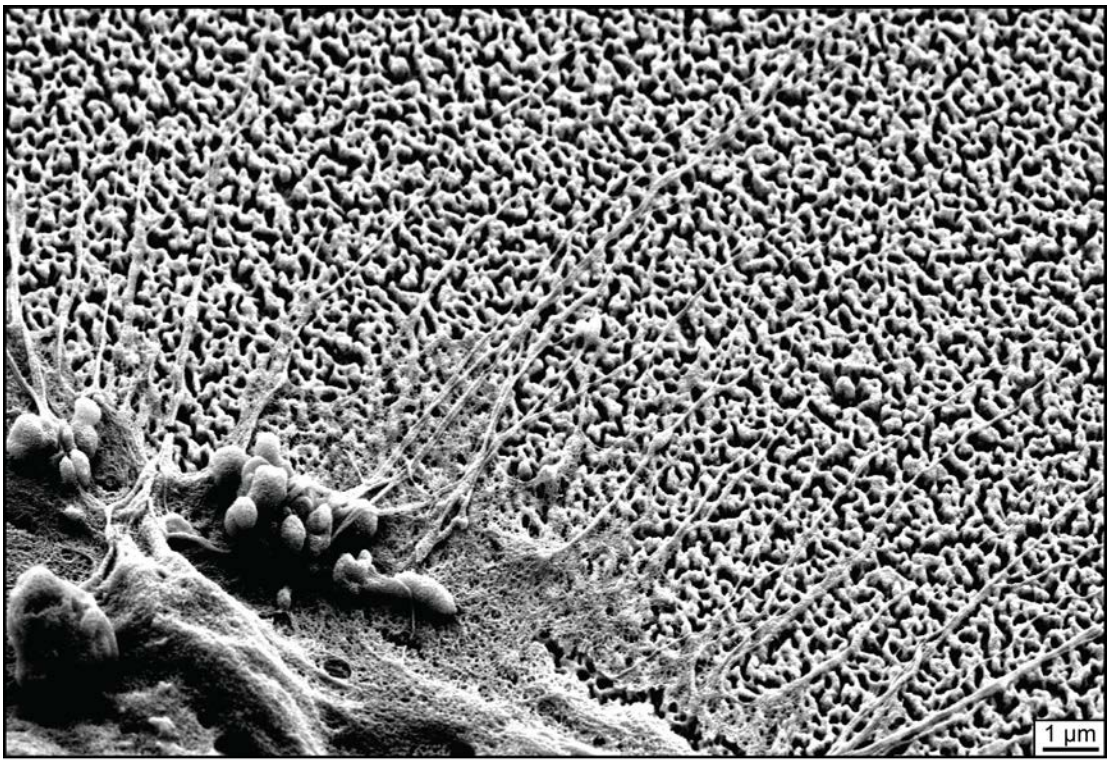

Figure S3. The SEM image illustrates that np-Au topography limits astrocytic morphology to the extension of fine and short processes spreading on continuous paths of ligaments.

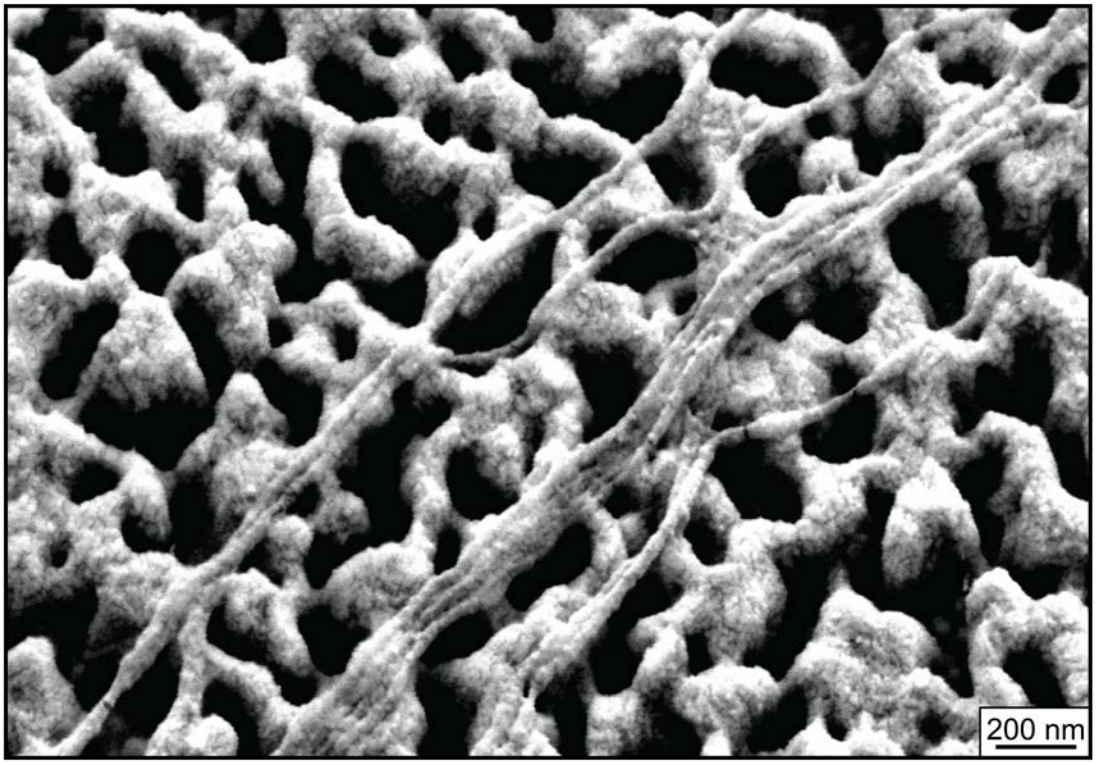

Figure S4. The SEM image illustrates the continuous path of ligaments that guide the growth of fine cellular processes.

Table S1. Average and Standard Deviations for Ligament Widths and Pore Diameters of Fabricated np-Au Films

Film	*Ligament Width (nm)*	*Pore Diameter (nm)*
Morphology 1	*30.62±18.94*	*87.11±65.55*
Morphology 2	*44.54±29.10*	*88.64±66.39*
Morphology 3	*70.65±52.34*	*149.20±104.07*
Morphology 4	*88.61±69.26*	*149.24±101.73*